



Microgel-based carriers enhance skeletal stem cell reprogramming towards immunomodulatory phenotype in osteoarthritic therapy

Pei-Lin Li^{a,b,1}, Da-Fu Chen^{c,1}, Xiao-Tong Li^{a,b,1}, Rui-Cong Hao^{a,b,1}, Zhi-Dong Zhao^{a,b,d}, Zhi-Ling Li^{a,b}, Bo-Feng Yin^{a,b}, Jie Tang^{a,b}, Yu-Wen Luo^c, Chu-Tse Wu^{a,b,**}, Jing-Jun Nie^{c,***}, Heng Zhu^{a,b,*}

^a Department of Stem Cells and Regenerative Medicine, Beijing Institute of Radiation Medicine, Road Taiping 27, Beijing, 100850, PR China

^b Beijing Key Laboratory for Radiobiology, Beijing Institute of Radiation Medicine, Beijing, 100850, PR China

^c Laboratory of Bone Tissue Engineering, Beijing Laboratory of Biomedical Materials, National Center for Orthopaedics, Beijing Research Institute of Traumatology and Orthopaedics, Beijing Jishuitan Hospital, Capital Medical University, Road Xijiekou 31, Beijing, 100035, PR China

^d People's Liberation Army General Hospital, Road Fuxing 28, Beijing, 100853, PR China

ARTICLE INFO

Keywords:

Microgel carriers
Skeletal stem cells
Immunomodulation reprogram
Single-cell RNA sequence
Osteoarthritis

ABSTRACT

Skeletal stem cells (SSC) have gained attentions as candidates for the treatment of osteoarthritis due to their osteochondrogenic capacity. However, the immunomodulatory properties of SSC, especially under delivery operations, have been largely ignored. In the study, we found that Pdpn⁺ and Grem1⁺ SSC subpopulations owned immunoregulatory potential, and the single-cell RNA sequencing (scRNA-seq) data suggested that the mechanical activation of microgel carriers on SSC induced the generation of Pdpn⁺Grem1⁺Ptgs2⁺ SSC subpopulation, which was potent at suppressing macrophage inflammation. The microgel carriers promoted the YAP nuclear translocation, and the activated YAP protein was necessary for the increased expression of Ptgs2 and PGE₂ in microgels-delivered SSC, which further suppressed the expression of TNF- α , IL-1 β and promoted the expression of IL-10 in macrophages. SSC delivered with microgels yielded better preventive effects on articular lesions and macrophage activation in osteoarthritic rats than SSC without microgels. Chemically blocking the YAP and Ptgs2 in microgels-delivered SSC partially abolished the enhanced protection on articular tissues and suppression on osteoarthritic macrophages. Moreover, microgel carriers significantly prolonged SSC retention time *in vivo* without increasing SSC implanting into osteoarthritic joints. Together, our study demonstrated that microgel carriers enhanced SSC reprogramming towards immunomodulatory phenotype to regulate macrophage phenotype transformation for effectively osteoarthritic therapy by promoting YAP protein translocation into nucleus. The study not only complement and perfect the immunological mechanisms of SSC-based therapy at the single-cell level, but also provide new insight for microgel carriers in stem cell-based therapy.

1. Introduction

Osteoarthritis (OA) is a degenerative whole-joint disease characterized by synovial inflammation and osteochondral lesions which leads to functional limitations and joint dysfunction [1,2]. Though numerous

risk factors including obesity, metabolism and genetics have been demonstrated to accelerate OA progression [1,2], increasing evidences show that macrophage derived inflammatory factors are positively correlated with articular cartilage destruction, osteophyte formation, and abnormal subchondral bone remodeling [3–6], which suggest the

Peer review under responsibility of KeAi Communications Co., Ltd.

* Corresponding author. Department of Stem Cells and Regenerative Medicine, Beijing Institute of Radiation Medicine, Road Taiping 27, Beijing, 100850, PR China.

** Corresponding author. Department of Stem Cells and Regenerative Medicine, Beijing Institute of Radiation Medicine, Road Taiping 27, Beijing, 100850, PR China.

*** Corresponding author.

E-mail addresses: 13910026365@163.com (C.-T. Wu), niejingjun_jst@126.com (J.-J. Nie), zhudingdingabc@163.com (H. Zhu).

¹ These authors contributed equally to this work.

<https://doi.org/10.1016/j.bioactmat.2023.12.022>

Received 9 October 2023; Received in revised form 13 December 2023; Accepted 23 December 2023

2452-199X/© 2023 The Authors. Publishing services by Elsevier B.V. on behalf of KeAi Communications Co. Ltd. This is an open access article under the CC BY-NC-ND license (<http://creativecommons.org/licenses/by-nc-nd/4.0/>).

chronic inflammation aggravates OA symptoms. Thus, inflammation-targeting strategies for OA treatment have gained increasing attention and yield promising effects [5,7,8].

Mesenchymal stem cells (MSC) are the type of mesenchyme-derived stem cells (MDSC) with powerful tissue regeneration properties and immunomodulatory capabilities, which contribute to the therapeutic effects on the settlement of immune disorders including chronic inflammatory joint disease such as OA [9,10]. However, increasing studies have emphasized the tissue specificity of MDSC. Skeletal stem cells (SSC) are tissue-specific MDSC in skeletons with the potential of osteogenesis and chondrogenesis [11–13]. Studies have demonstrated that the activated SSC in subchondral bones benefits the regeneration of murine articular cartilage [14,15], which contribute to the application of SSC for OA treatment. Moreover, most of the current studies attribute the osteochondral regeneration of SSC to their differentiation properties, and the immunoregulatory properties of SSC have been largely ignored.

Except for the cell types, recent studies also confirm the importance of carriers for MDSC-based therapy. Gelatin-microniches applied for human MSC delivery not only protect the loaded cells from non-essential mechanical damage during operation, but also significantly improve cell retention, survival, and regenerative effects *in vivo* for the treatment of critical limb ischemia [16]. In addition, human pluripotent stem cells cultured in microniches are also proved to tend to differentiate into endothelial cells and exhibit enhanced vascular repairing capacity in the model of critical limb ischemia [17]. Microcarriers play important role in stem cell-based therapy, however, most research focuses on the effects of microniches/microgels in the functional phenotype of stem cells, the immunomodulatory capacity of stem cells and the contribution of cell subpopulation alteration to the immunomodulatory phenotype of microniches/microgels-delivered stem cells have rarely been explored.

Herein, the microgels based delivery system for SSC was constructed in the present study. The immunoregulatory capacity of SSC, and the reprogramming effects of microgel carriers on the SSC subpopulation alteration and immunomodulatory phenotype were studied by single-cell transcriptomic and functional analysis. We found that not all cell subpopulations respond to the mechanical reprogramming effects of microgels and possessed the immunoregulatory potentials. Among the obtained cell subpopulations, Pdpn⁺ SSC and Grem1⁺ SSC showed the immunomodulatory potential and plasticity. Moreover, microgel carriers enhanced the mechanical properties of SSC via promoting YAP nuclear translocation, which altered the cell fate of Pdpn⁺ SSC and Grem1⁺ SSC in microgels, resulting in the emergence of an immunoregulatory SSC subpopulation (Pdpn⁺Grem1⁺Ptgs2⁺ SSC). The immunomodulatory SSC subpopulation enhanced the overall immunomodulatory capacity of microgels-delivered SSC to improve the therapeutic effects in OA treatment by suppressing OA macrophage inflammation. Our study provides profound insights into the role of microgel-based cell carrier in YAP activation and cell subpopulation alteration, which further result in the enhanced SSC immunomodulation and alleviating OA osteochondral damages. The work offers a promising strategy and systematic immunological mechanisms studies at the single-cell level for the development of SSC-based osteochondral tissue-engineering applications.

2. Materials and methods

2.1. Animals

8-week-old (n = 100) and 1-week-old (n = 20) SPF Sprague Dawley (SD) rats were purchased from Beijing Vital River Laboratory Animal Technology Co, Ltd. China. All animal studies were conducted in accordance with the ethics committee of the Academy of Military Medical Science (Number: IACUC-DWZX-2020-765).

2.2. Harvesting and culture of SSC

SSC were harvested from femur and tibia according to our previously reported procedure [18]. Briefly, long bones were dissected from 1-week-old SD rats, and bone marrow cells were flushed out, and then the long bones were shredded and digested by collagenase II (Sigma U. S., 0.1 % g/mL) for 30 min in the 37 °C incubator. After digestion, the bone fragments were cultured in alpha modification-minimum essential medium (α -MEM; Invitrogen) with 10 % fetal bovine serum (FBS; Pricella). The adherent cells (SSC) from passages 2 to 5 were used.

In order to construct microgels-based delivery system for SSC (SSC with microgels), the gelatin porous microgels was used based on the established cryogelation method [19]. SSC were resuspended at a concentration of 5×10^6 cells/mL. Then, 200 μ L SSC suspension was seeded on one microgel tablet (20 mg, 3D Table Trix, CytoNiche Biotechnology), and then cultured for 2 h in the 37 °C incubator. After that, phosphate buffer saline (PBS) or complete medium was added for subsequent experiments.

2.3. Bulk RNA sequencing (RNA-seq) of SSC

To investigate the reprogramming property of SSC with microgel, aliquots (2×10^5 /well) SSC suspensions with or without microgel carriers were seeded on six-well culture plates and cultured for 3 days, and then RNA-seq analysis was performed. The mRNA library constructing and sequencing were conducted at GENEWIZ, Inc (Suzhou, China). Total RNA was utilized for library construction, and the libraries with different indexes were multiplexed and loaded on an Illumina Novaseq instrument for sequencing by using a 2×150 paired-end (PE) configuration according to manufacturer's protocols.

2.4. Single-cell RNA sequencing (scRNA-seq) of SSC

To investigate the cellular heterogeneity of SSC and explore the immunoregulatory potential and plasticity of SSC in microgels at single-cell resolution, SSC suspensions with or without microgel carriers were harvested. The scRNA-seq libraries were prepared by using the Chromium Single Cell 3' Reagent Kits v3 ($10 \times$ Genomics) at Berry Genomics Corporation (Beijing, China). Briefly, the single cells of SSC with or without microgel carriers were washed with PBS and resuscitated to a concentration of 800~1000 cells/ μ L (viability ≥ 90 %), and then cells were captured in droplets to generate single cell gel beads-in-emulsion (GEMs). After the reverse transcription step, GEMs were broken and barcoded-cDNA was purified with Dynabeads, and then PCR amplification was performed. Then the 3' gene expression library was constructed by using amplified cDNA. Subsequently, amplified cDNA was fragmented and end-repaired, double-size selected with SPRIselect beads, and sequenced on an Illumina NovaSeq platform to generate 150 bp paired-end Reads.

2.5. Generation and analysis of scRNA-seq data

The raw data of scRNA-seq were processed with Cell Ranger (version 7.0) ($10 \times$ Genomics) and aligned to the rat genome constructed by the cellranger-mkref function. Further analyses were carried out in R (version 4.1.0) by using Seurat (version 4.2.0; <https://satijalab.org/seurat/>). For data preprocessing, cells with fewer than 200 detected genes or greater than 7500 genes were excluded, and less than 15 % of mitochondrial gene were retained. Cell doublets were removed using R package Doublet Finder. After filtering, 9232 cells from SSC and 12177 cells from SSC with microgels were analyzed. For integrated analysis of SSC datasets with or without microgel, we used canonical correlation analysis (CCA) method implemented in Seurat. For cell clustering, a Shared Nearest Neighbor (SNN) Graph was conducted by FindNeighbors function with a resolution of 1.5. Uniform manifold approximation and projection (UMAP) was used to create a 2D map. For the analysis of

differentially expressed genes, the FindAllMarkers function of Seurat was performed to identify differentially expressed genes in SSC (Table S1) and SSC with microgels (Table S2).

2.6. Gene ontology (GO) and gene set enrichment analysis (GSEA)

For the GO and GSEA of SSC datasets with or without microgels, R package ClusterProfiler (version 4.2.2; <https://guangchuangyu.github.io/software/clusterProfiler/>) were used.

2.7. Kyoto encyclopedia of genes and genomes (KEGG) pathway analysis

KEGG pathway analysis was performed by using the DAVID website (<https://david.ncifcrf.gov/tools.jsp>), and visualization was done by using ggplot2 (version 3.4.1; <https://ggplot2.tidyverse.org/>)

2.8. Single cell trajectory analysis

RNA velocity analysis was performed by using velocity (version 0.17; <https://github.com/velocyto-team/velocyto.py>) and scVelo (version 0.2.3; <https://github.com/theislab/scvelo>). To generate the loom files, the run10 × function of velocity was conducted on Cellranger outputs files, and scVelo functions were applied to calculate the root and terminal states. For the PAGA analysis, the python package Scanpy (version 1.9.1; <https://github.com/theislab/scanpy>) was utilized.

2.9. Cell communication analysis

R package CellChat (version 1.1.3; github.com/sqjin/CellChat) was used for cell communication analysis. For the pattern of cellular communication, we used the “ECM-Receptor” pattern to analyze the main cell population with significant mechanical properties.

2.10. Multilineage differentiation assay

Osteogenic, chondrogenic, and adipogenic differentiation of SSC were performed as our reported protocol [18]. For osteogenesis assay, SSC suspensions with or without microgel carriers were seeded into 48-well plates and cultured in stem cell growth medium (α -MEM with 10 % FBS) or osteogenic culturing medium (50 μ M ascorbate-2-phosphate, 10 mM β -glycerol phosphate and 10^{-7} M dexamethasone). After 14 or 28 days of culturing, alkaline phosphatase (ALP) staining and von Kossa staining were executed. For chondrogenesis assay, SSC suspensions with or without microgel carriers were seeded into 48-well plates and cultured in stem cell growth medium or chondrogenic culturing medium (50 μ M ascorbate-2-phosphate, 0.1 mM dexamethasone, 50 μ g/mL proline, 1 % ITS (1 ×), 1 mM sodium pyruvate and 20 ng/ml TGF- β 3). After 21 days of culturing, toluidine blue staining was executed. For adipogenesis assay, SSC suspensions with or without microgel carriers were seeded into 48-well plates and cultured in stem cell growth medium or adipogenic culturing medium (0.5 μ M 3-Isobutyl-1-methylxanthine, 10^{-6} M dexamethasone and 10 ng/ml insulin). After 14 days of culturing, Oil Red O staining was conducted.

2.10.1. Scanning electron microscopy (SEM) and energy-dispersive spectroscopy (EDS)

The samples were washed with PBS and fixed in 4 % PFA. Then, the samples were transferred into 1 % OsO₄ in PBS for 1–2 h at room temperature. After that, the samples were sequentially dehydrated in 30 %, 50 %, 70 %, 80 %, 90, 95 % and 100 % ethanol. Subsequently, the samples were dried and attached to metallic stubs using carbon stickers, and were sputter-coated with gold for 30s. Afterwards, the samples were observed with a scanning electron microscope (HITACHI, SU8100). The EDS measurements were performed by AZtec X-Max 80.

2.11. Particle size analysis

The particle size distribution analysis was conducted by using ImageJ software (version: ImageJ 1.53c).

2.12. Cell proliferation and viability

The ability of proliferation was evaluated by the Cell Counting Kit 8 (CCK-8; Dojindo, Japan). The cell suspensions of SSC with or without microgel carriers were seeded into 96-well plate. CCK-8 solution was added into growth medium at a ratio of 1:10, and then the plates were cultured for 2 h in the 37 °C incubator. After incubation, the supernatant was sucked out to the empty 96-well culture plate and absorbance was detected by using a microplate reader at a wavelength of 450 nm. The CCK-8 tests were conducted on days 1, 4, 7, and 10. For graded numbers of SSC incubated on microgel carriers, 1×10^5 , 1×10^6 and 2×10^6 SSC were respectively incubated with one microgel tablet (20 mg), and cultured for 2 h in the 37 °C incubator. Then, one-tenth of the supernatant of graded numbers of SSC with microgel carriers were used for each test of CCK-8.

The viability of SSC with or without microgel carriers was detected on days 1, 4, 7 and 10 by live/dead assay with Calcein/PI Cell Viability/Cytotoxicity Assay Kit according to the manufacturer’s protocol (Beyotime) and visualized by a fluorescence microscope (Olympus CKX53).

2.13. Colony-forming unit fibroblast formation assay (CFU-F assay)

The self-renewal capacity of SSC with or without microgels was performed by CFU-F assay. Aliquots (5×10^2 /well) of SSC suspensions with or without microgels were seeded into six-well plates and cultured for 7 days. To assess the colony formation, crystal violet staining was conducted.

2.14. Real-time qPCR and ELISA

SSC with or without microgel carriers were seeded into 6-well plates and cultured for 3 days. In some groups, SSC was incubated in microgels, and then respectively cultured in growth medium with 1 μ M YAP inhibitor (verteporfin) and in growth medium with 10 μ M COX2 inhibitor (NS-398) for 3 days in six-well culture plates, respectively. The cell and culture medium were collected for qPCR and ELISA. The rat monocytes, isolated from the bone marrow of femurs and tibias, were divided into 6 groups: (i) monocytes cultured in growth medium (monocytes); (ii) monocytes cultured in growth medium containing 20 ng/mL TNF- α (macrophages); (iii) monocytes cultured in growth medium containing 20 ng/mL TNF- α and 10 % SSC supernatant (macrophages + SSC medium); (iv) monocytes cultured in growth medium containing 20 ng/mL TNF- α and 10 % cell supernatant of SSC with microgels (macrophages + (SSC with microgel) medium); (v) monocytes cultured in growth medium containing 20 ng/mL TNF- α and 10 % cell supernatant of SSC with microgel + verteporfin group (macrophages + (SSC with microgel + verteporfin) medium); (vi) monocytes cultured in growth medium containing 20 ng/mL TNF- α and 10 % cell supernatant of SSC with microgel + NS-398 group (macrophages + (SSC with microgel + NS-398) medium). All groups were cultured for 3 days in six-well culture plates, and the cells and culture medium were collected for qPCR and ELISA. The qPCR procedure were performed as previously reported. The rat GAPDH, Ptg2, TNF- α , IL-1 β and IL-10 primers were synthesized by Tsingke Biotechnology and were shown in Table S3. Rat PGE₂ in SSC supernatants and TNF- α , IL-1 β , and IL-10 in monocyte supernatants were detected by ELISA according to manufacturer’s protocols (Czkwbio, China). Optical density was detected by using a microplate reader at a wavelength of 450 nm.

2.15. Western blotting

The total protein was extracted by protein lysis buffer (BioRad, Hercules, California) according to manufacturer's protocols. And then proteins were resolved via 10 % sodium dodecyl sulfate polyacrylamide gel electrophoresis (SDS-PAGE) and transferred to nitrocellulose membranes. The membranes were incubated with anti-vinculin (proteintech, 1:5000), anti-phospho-YAP (CST, 1:2000), anti-YAP (CST, 1:2000), anti-COX2/Cyclooxygenase 2/Ptgs2 (proteintech, 1:1000), anti-Lamin b1 (proteintech, 1:2000) and anti-GAPDH (CST, 1:2000) at 4 °C for 8–12 h. After that, the membranes were incubated with horseradish peroxidase (HRP)-conjugated goat anti-rabbit IgG (Servicebio, 1:3000) or HRP-conjugated goat anti-mouse IgG (Servicebio, 1:3000) at room temperature for 1 h.

2.16. Immunofluorescence staining

The samples were washed with PBS, fixed with 4 % paraformaldehyde for 30 min, according to experimental requirements, were incubated with anti-Pdpr (proteintech, 1:200), anti-Grem1 (CST, 1:50), anti-Cd200 (proteintech, 1:200), anti-Ctsk (Abcam, 1:200), anti-Ptgs2 (proteintech, 1:200), anti-vinculin (proteintech, 1:200) or anti-YAP (CST, 1:200) at 4 °C for 8–12 h. After that, samples incubated with goat anti-rabbit IgG (Servicebio, Alexa Fluor 488, 1:300), goat anti-rabbit IgG (Servicebio, Cy3, 1:300) or goat anti-mouse IgG (Servicebio, Alexa Fluor 488, 1:200) for 1 h at room temperature. Nuclear staining was conducted with DAPI (Sigma), and F-actin stained by rhodamine phalloidin (Beyotime). Tissue samples were fixed in 4 % paraformaldehyde. After decalcification, all samples were embedded in paraffin and sectioned at 6- μ m slices. The tissue sections were immunofluorescently stained with primary antibodies targeting Sry (Santa Cruz, 1:200), CD11b (Servicebio, 1:500), TNF- α (Uscn Life Science Inc., 1:1000), IL-1 β (Servicebio, 1:1200) and IL-10 (Servicebio, 1:1000), and the goat anti-rabbit IgG (Servicebio, Alexa Fluor 488, 1:400) and goat anti-rabbit IgG (Servicebio, Cy3, 1:500). DAPI was used to stain the nuclei. The images were observed by a fluorescence microscope (Olympus CKX53) or Nikon confocal microscope (Nikon).

2.17. Rheological property evaluation

The injectability of SSC with microgels was evaluated by rheological experiments, conducted at 37 ± 5 °C in the straincontrolled mode. The strain sweep experiments were performed in the range of 0–100 % strain at a frequency of 1 rad/s.

2.18. Transplantation of SSC into a rat OA model

SD rats (8-week-old) were divided into 6 groups: sham (n = 8), OA + SSC (n = 8), OA + SSC with microgels (n = 8), OA + SSC with microgels + verteporfin (n = 8) and OA + SSC with microgels + NS-398 (n = 8). OA of knee joint was induced by transection of anterior cruciate ligament (ACL). Anesthetized rats and surgically transected the ACL to induce knee instability. For sham group, only the articular cavity was exposed, then sutured and no anterior cruciate ligament was cut. For OA + SSC, SSCs were injected at 1×10^5 cells/knee. For OA + SSC with microgel, OA + SSC with microgels + verteporfin and OA + SSC with microgels + NS-398 groups, 1×10^5 SSCs in about 2 mg microgels with 100 μ L PBS were injected; before injection, SSC was incubated on microgel, and then cultured in growth medium, medium containing 1 μ M YAP inhibitor (verteporfin) and medium containing 10 μ M COX2 inhibitor (NS-398), respectively, for 3 days in six-well culture plates.

2.19. Transplantation of SSC in vivo and bioluminescence imaging

To track SSC with or without microgels *in vivo*, the cells were infected by lentiviruses with firefly luciferase (Luc+). Then both free Luc + SSC

and Luc + SSC with microgels were injected into the knee joints of OA rats. OA rats were divided into two groups: (i) 1×10^5 SSC were injected into the knee joints of OA models; (ii) 1×10^5 SSC with microgels were injected into the knee joints of OA models. Bioluminescence imaging was conducted to track the retention of SSC with or without microgels on days 1, 4, 7, and 12 after injection by using a Xenogen IVIS LuminaII imaging system (Caliper Life Sciences).

2.20. Degradation experiment of microgel carriers in vitro

Microgel carriers were cultured in growth medium with 20 ng/mL TNF- α , 20 ng/mL IL-1 β and 100 ng/mL MMP1 in the 37 °C incubator. Then, the degradation of microgel carriers were observed by an optical microscope on days 1, 4, 7 and 12 (Olympus CKX53).

2.21. Microcomputerized tomography (μ CT) analysis

For μ CT analysis, the rats were killed at 4 weeks and knee joints were harvested. All samples were fixed in 4 % paraformaldehyde, and scanned by a μ CT system (Scanco Medical, Bassersodrf, Zurich, Switzerland). A scanning time of 14 min with settings of 70 kVp and 114 μ A was used. The imaging reconstruction of 3D images was conducted using a standard convolution back-projection. The degree of OA changes was assessed by the number of osteophyte and the degree of joint destruction [20].

2.22. Histological examination and immunohistochemistry

For histology analysis and immuno-staining, all samples were fixed in 4 % paraformaldehyde. After decalcification, all samples were embedded in paraffin and sectioned at 6- μ m slices. HE staining was conducted to observe the structure of articular tissues. Toluidine blue and safranin-o/fast green stainings were performed to evaluate the cartilaginous matrix distribution. In addition, the expression of collagen type I and collagen type II was detected by immunohistochemical assay with anti-Col1a1 (Servicebio, 1:800) and anti-Col2a1 (Abcam, 1:500), respectively.

2.23. Statistical analysis

For all quantitative results, three replicate samples were performed at least. Data were presented as means \pm SDs. To detect the significance of differences, the Student's *t*-test or one-way ANOVA was applied. *P* value < 0.05 was considered to be statistically significant.

3. Results

3.1. Preparation and viability of SSC with or without microgel carriers

Commercially available microgels were used for SSC delivering. The scanning electron microscopy (SEM) images showed microgels were dispersed porous spherical microcarriers with the diameter of about 100–110 μ m (Fig. 1A and B). To explore a suitable SSC-microgels culture system, graded numbers of SSC, obtained from the long bones of one-week-old SD rats (Fig. 1C), were incubated with microgels (Fig. 1D). The CCK-8 assays were performed at days 1, 4, 7 and 10. The CCK-8 data showed that cell viability of 1×10^6 group were better than that of 2×10^6 group and 1×10^5 group at day 10, which suggested an appropriate number of SSC (1×10^6) for cultivation on microgel carriers (Fig. 1E). In addition, SSC with or without microgel carriers were observed through SEM. The data showed that SSC cultured on cell culture dishes exhibited a flat morphology (Fig. S1A), while SSC with microgels grew into the pores of microgel carriers (Fig. 1F). Subsequently, the cell viability of SSC with or without microgel carriers were examined. The live/dead staining showed SSC had better cell viability in microgels (Fig. 1G and Fig. S1B). However, SSC cultured on flat surfaces exhibited mild cell

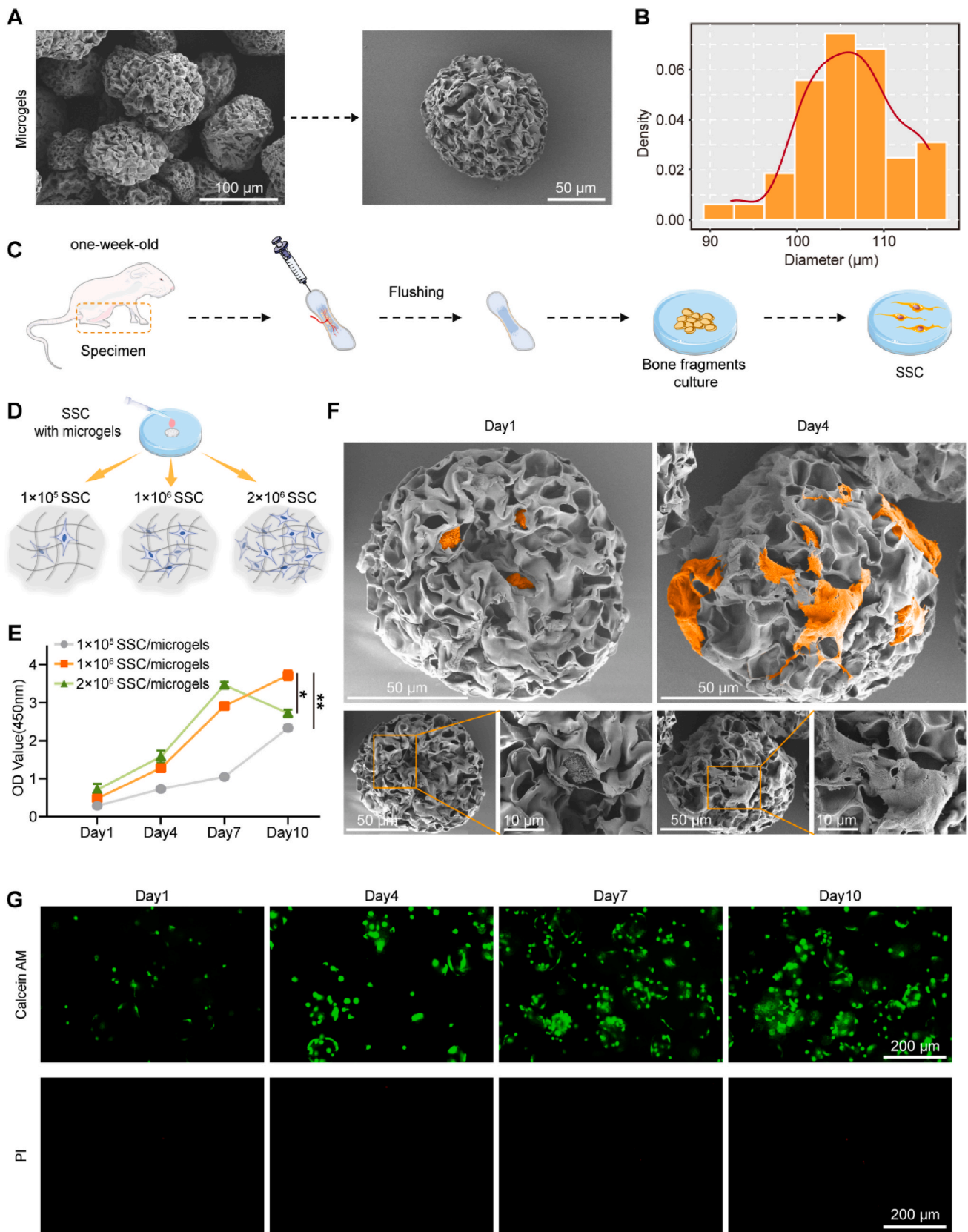


Fig. 1. Characterization of SSC in microgel carriers. (A) The porous ultrastructure of the microgel carriers shown by SEM images. (B) Density plot of size distribution of the microgel carriers. (C) Schematic illustration of the SSC acquisition. (D) Schematic illustration of SSC incubation in microgel carriers. (E) CCK-8 assay showing the proliferation activity of different numbers of SSC in microgel carriers. (F) SEM images showing the morphology of SSC in microgel carriers at days 1 and 4. SSC were marked by orange color. (G) Live/dead cell staining showing the cell viability of SSC in microgel carriers at days 1, 4, 7 and 10. * $p < 0.05$, ** $p < 0.01$. All tests were replicated at least three times.

death (Fig. S1C).

3.2. SSC delivered with microgel carriers enhanced OA therapeutic efficacy by reducing osteo-chondral lesions

For OA treatment, SSC with or without microgels were intra-articularly administered as reported previously [21,22]. The SEM and energy-dispersive spectroscopy (EDS) of the microgels before and after injection were performed to determine whether the injection behavior affects the morphology and composition of the microgels. The results showed that the microgels is composed of four major elements carbon, oxygen, nitrogen and sulfur, and there was no significant changes of the morphology and composition of microgels before and after injection have been observed (Fig. 2A, B, C). Besides, the injectability of microgel carriers and SSC delivered with microgels were detected by rheological experiments. The strain amplitude sweep results, showing the storage moduli (G') and loss moduli (G'') of the microgels with or without SSC, revealed that both microgels and SSC with microgels could sustain up to 80 % compressive strain (Fig. 2D). However, in the strain range of less than 80 %, the stress of SSC with microgels was consistently lower than that of microgels (Fig. 2E). These data showed the superior elasticity of SSC-microgels under compression than that of microgels, which suggested SSC-microgels was an efficient delivery system.

To explore the *in vivo* survival and distribution of SSC with or without microgels after intra-articular injection, Sry immunofluorescence and bioluminescence imaging were performed. The results of Sry immunofluorescence showed that neither SSC nor SSC delivered with microgels was implanted into OA joints after intra-articular injection (Fig. S2A). Bioluminescence imaging showed the survival time of SSC with microgels *in vivo* was significantly longer than that of SSC (Figs. S2B and C), suggesting that the SSC with microgels delivery system might protect SSC from insults in the pathological microenvironment of OA joints. In addition, the data of degradation experiments showed that microgel carriers significantly degraded in the presence of inflammatory factors that contribute to OA lesions at day 12 (Figs. S2D and E).

The overall efficacy of SSC with or without microgels on OA treatment was evaluated by μ CT and histological analysis (Fig. 2F). μ CT imaging data showed remarkably irregular articular surface and osteophyte formation in the knee joints of OA rats, while SSC with microgels injection significantly attenuated the osteochondral lesions compared with SSC group (Fig. 2G). In addition, μ CT-based OA grading of all individuals showed that the SSC with microgels yielding better protective effects (Fig. 2H). Consistent with the μ CT results, histological staining data showed that SSC with microgels resulted in less cartilage destruction (Fig. 2I), lower Mankin score (Fig. 2J), higher expression of type II collagen (Fig. 2K), and lower expression of type I collagen (Figs. S3A and B), suggesting an strengthened protective effects on the cartilage structure and extracellular matrix. Also, it was worth noting that the microgels did not have an therapeutic effect on OA (Figs. S3C and D).

Together, these results demonstrated that the SSC with microgels delivery system had stronger advantages in OA treatment.

3.3. Microgel carriers delivery enhances the immunomodulatory capacity of SSC

To further investigate the regulations of microgel carriers on SSC, the cell proliferation, selfrenewal and multiple-differentiation of SSC with or without microgel carriers were explored. The results of CCK-8 assays indicated that microgels cultivation significantly promoted the cell proliferation of SSC at least at day 7 and 10 (Fig. S4A), while CFU-F assay data proved that there was no significant difference in the self-renewal between SSC and SSC with microgels (Figs. S4B and C). In addition, trilineage differentiation assays showed that the osteogenic, chondrogenic and adipogenic potential of SSC and SSC with microgel carriers did not remarkably changed in the present study (Fig. S4D).

Alternations of SSC properties in microgels were also explored by

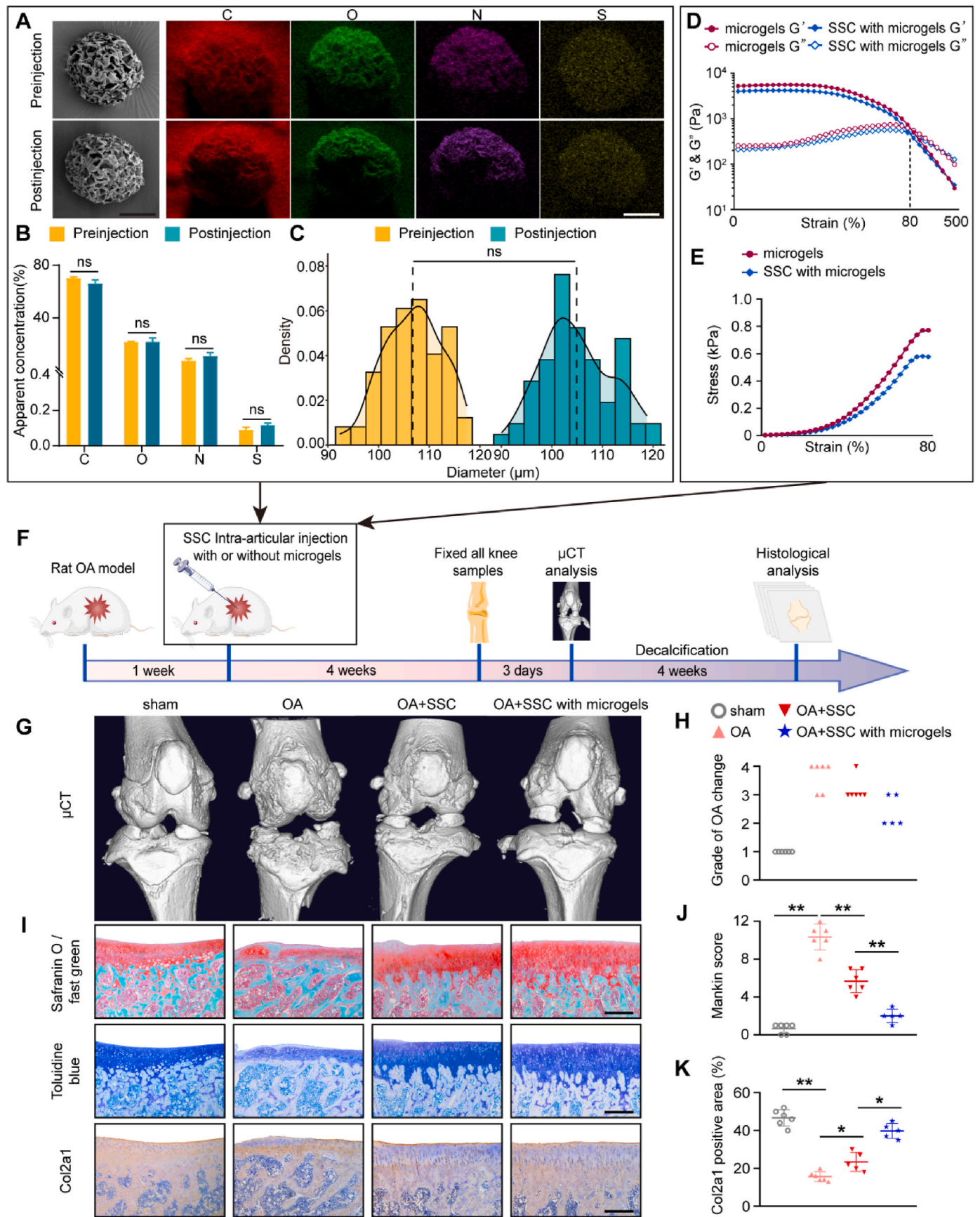
bioinformatic analyses. The bulk RNA-seq was performed to compare the gene expression profiles of SSC and SSC with microgels. There were 1528 differentially expressed genes (DEGs) in SSC with microgels compared with SSC, including 747 upregulated genes and 781 down-regulated genes (Figs. S5A and B). GO analysis showed that the up-regulated DEGs in SSC with microgels were significantly enriched in regeneration and immunomodulation (Fig. 3A), among which the representative DEGs were shown in Fig. S5C. Moreover, gene set enrichment analysis (GSEA) of all DEGs showed that SSC with microgels exhibited an enhanced ability to regulate myeloid cell differentiation (Fig. 3B). Notably, convincing evidence has demonstrated that over-activated macrophages aggravate OA inflammation, leading to progressive destruction of joint tissues [23,24]. Our previous work also has demonstrated that reducing the inflammation of macrophages alleviates OA symptoms [9]. Therefore, SSC with microgels might reduce OA macrophage inflammation through immunomodulatory capacity to achieve better therapeutic effects. The qPCR results of OA tissues confirmed that SSC with microgels yielded strengthened suppression on the expression of macrophage-derived inflammatory factors such as TNF- α and IL-1 β , and promoted the expression of the anti-inflammatory factor such as IL-10 (Fig. 3C). Correspondingly, immunofluorescence staining of OA tissues showed that SSC with microgels injection resulted in significant reductions in CD11b⁺TNF- α ⁺ and CD11b⁺IL-1 β ⁺ macrophages compared with the SSC group, while CD11b⁺IL-10⁺ macrophages significantly increased (Fig. 3D), suggesting that SSC with microgels had stronger ability to suppress inflammatory macrophages *in vivo*.

In brief, these results showed that the SSC with microgels efficiently enhanced the immunomodulatory capacity compared with SSC.

3.4. Microgel carriers enhanced SSC reprogramming towards immunomodulatory phenotype via inducing Pdpn⁺ Grem1⁺ Ptg2⁺ SSC subpopulation

To further elucidate the effects of microgel carriers on the cellular composition and functional phenotype of SSC, single-cell suspensions of SSC and SSC delivered with microgels were generated for scRNA-seq (Fig. 4A). We first analyzed the single-cell data of SSC cultured on flat surfaces. Four distinct clusters were identified based on the most significantly expressed genes (Figs. S6A and B). SSC1 (*Pdpn*, *Spp1*, *Acan*, and *Col18a1*), SSC2 (*Grem1*, *Grem2*, *Mylk* and *Gpx3*), SSC3 (*Cd200*, *Igf1*, *Cacnb2*, and *Cdh2*) and SSC4 (*Ctsk* and *Runx2*) respectively expressed classical SSC markers Pdpn [13], Grem1 [12], Cd200 [11] and Ctsk [25] (Fig. S6C). Consistent with the scRNA-seq data, immunofluorescent staining confirmed the presence of the four subclusters in SSC (Fig. S6D). The DEGs of each group were used for GO analysis. All four clusters were capable of osteogenic and chondrogenic differentiation, but SSC1 showed stronger ability of anti-apoptosis; SSC2, 3, 4 were significantly active in BMP, NOTCH and PDGF signaling pathways, respectively (Fig. S6E). Notably, SSC1 (Pdpn⁺ SSC) and SSC2 (Grem1⁺ SSC) had potential immunomodulatory ability and stronger stem cell property (Fig. S6E). Furthermore, single-cell trajectory analysis including RNA velocity and PAGA also revealed that SSC1 and SSC2 had the ability of differentiating into other SSC subsets (Figs. S6F and G). These results indicated that SSC was multipotent and heterogeneous, and Pdpn⁺ SSC and Grem1⁺ SSC had stronger plasticity in immunomodulation and stemness.

After integration analysis, we obtained 5 subpopulations in microgels-delivered SSC, and a newly emerged subpopulation (SSC5) accounted for about 70 % to the total number of microgels-delivered SSC (Fig. 4A and B). Moreover, SSC5 highly expressed *Pdpn* and *Grem1* (Fig. 4C), suggesting that SSC5 may be derived from SSC1 (Pdpn⁺ SSC) and SSC2 (Grem1⁺ SSC). Consistently, the results of RNA velocity and PAGA also indicated the two origins (SSC1 and SSC2) of SSC5 (Fig. 4D and E). Gene expression heatmap showed that the feature genes of SSC1 were down-regulated along pseudotime trajectory 1 (Fig. 4F), the highly



(caption on next page)

Fig. 2. Analysis of efficacy of SSC with or without microgel carriers for OA treatment. (A) SEM images of the microgel carriers before and after injection, and the distribution of carbon, oxygen, nitrogen and sulfur on microgel carriers were shown by EDS. (B) The apparent concentration of each element of the microgels before and after injection. (C) Density plot of size distribution of the microgel carriers before and after injection. The dashed line represents the average of diameter. (D–E) Strain amplitude sweep (D) and stress-strain curves (E) of the microgel carriers with or without SSC. (F) The workflow of OA treatment by SSC with or without microgels and their efficacy evaluation. (G) μ CT analysis of OA articular tissues in different treatment groups at 4 weeks after intra-articular injection. (H) OA grade change in each treatment group at 4 weeks after injection. (I) Safranin O/fast green staining (top), toluidine blue staining (middle) and Col2a1 immunohistochemical staining (bottom) of OA articular tissues in different treatment group at 4 weeks after injection. Scale bars: 200 μ m. (J) Mankin scores of each treatment group at 4 weeks after injection. (K) Semi-quantitative analysis of Col2a1 immunohistochemical staining for each treatment group at 4 weeks after injection. All tests were replicated at least three times. * $p < 0.05$, ** $p < 0.01$, ns, no significance. For the treatments of OA rats, $n \geq 5$ per group.

expressed genes in SSC2 were down-regulated along pseudotime trajectory 2 (Fig. 4G), and the feature genes of SSC5 were up-regulated along both pseudotime trajectory 1 and 2, including numerous immunomodulatory genes (*Sfrp1*, *Tnfrsf6*, *Ptgs2*, *Nfkbia*, *Ccl2* and *Ccl7*), especially *Ptgs2* (Fig. 4F and G). Thus, the novel subset SSC5 was defined as $\text{Pdpn}^+\text{Grem1}^+\text{Ptgs2}^+$ SSC due to its origin and co-expression of *Pdpn* or *Grem1* with *Ptgs2* (Fig. 4F, G and Fig. S7). Notably, these feature genes varying with pseudotime 1 and pseudotime 2 were differentially expressed in SSC and SSC delivered with microgels. The feature genes (especially *Ptgs2*) at the end of pseudotime trajectory 1 and 2 were more strongly expressed in the SSC with microgels group, which indicated that the emergence of the novel subpopulation ($\text{Pdpn}^+\text{Grem1}^+\text{Ptgs2}^+$ SSC) might be attributed to microgels cultivation (Fig. 4H and I). Correlation analysis of each subpopulation showed the independency of the novel subset ($\text{Pdpn}^+\text{Grem1}^+\text{Ptgs2}^+$ SSC) compared with other subpopulations, suggesting its unique function (Fig. 4J). Gene expression analysis showed that the immunomodulatory genes were highly expressed in SSC5 (Fig. S8). To further explore the characteristics of SSC5, GO analysis was performed, and the data showed that SSC5 possessed immunomodulatory properties (including negative regulation of immune system process and regulation of macrophage activation) and mechanical stimuli-responsive characteristics (including focal adhesion assembly and actin cytoskeleton reorganization) (Fig. 5A). In addition, KEGG pathway analysis indicated that the “ECM-receptor interaction”, which has been reported to promote focal adhesion protein activation and cytoskeletal reorganization [26], were significantly activated in microgels-delivered SSC (Fig. S9A), so we used the “ECM-Receptor” pattern of CellChat R package for analysis to explore the ECM-related mechanical effects on SSC5. Compared with 2D-cultured counterpart, the “ECM-Receptor” pattern had stronger interaction weights in microgels-delivered SSC (Fig. 5B), and the significantly strengthened signaling patterns of SSC5 included COLLAGEN, FN1 and TENASCIN pathways (Fig. 5C and Fig. S9B). Also, GO analysis showed that the ligand and receptor genes of these signaling pathways (Figs. S9C, D, E) were enriched in functions including secretory activity and immunomodulation (Fig. 5D), which indicated that mechanical reprogramming induced the generation of immunomodulatory subset (SSC5) in microgel carriers. Importantly, *Ptgs2*, the immunomodulatory feature gene of SSC5, had more interactions with mechanical property and macrophage regulation gene set (Fig. 5E).

Together, these results suggested that mechanical reprogramming of the microgel carriers activated the overall immunomodulatory capacity of SSC by generating SSC5 ($\text{Pdpn}^+\text{Grem1}^+\text{Ptgs2}^+$ SSC) with mechanical and immunomodulatory properties.

3.5. Microgel carriers induced $\text{Pdpn}^+\text{Grem1}^+\text{Ptgs2}^+$ SSC subpopulation via promoting YAP nuclear translocation

Considering that our scRNA-seq data suggested SSC5 ($\text{Pdpn}^+\text{Grem1}^+\text{Ptgs2}^+$ SSC) was a mechanosensitive subpopulation with focal adhesion assembly and actin cytoskeleton reorganization in microgels-delivered SSC (Fig. 5A), we further explored the effects of microgel carriers on the mechanical properties of SSC. Immunofluorescence staining showed increased vinculin (VCL) activity in the SSC with microgels group (Fig. 6A and B). Additionally, the results of western blotting showed the enhanced total protein expression of VCL in

microgels-delivered SSC (Fig. 6E). Moreover, Yes-associated protein (YAP), a mechanosensitive transcriptional activator, has been reported to be associated with focal adhesion assembly and actin cytoskeleton reorganization [26,27]. The immunofluorescent staining also showed higher nuclear translocation of YAP in microgels-delivered SSC (Fig. 6C and D). Of note, the data of western blotting analysis revealed weakened total protein expression of phospho-YAP (p-YAP), strengthened expression of nuclear YAP protein, and no significant change in the total protein expression of YAP in the SSC with microgels group (Fig. 6E), indicating YAP nuclear translocation increased in microgels-delivered SSC. These results showed that microgels indeed enhanced the mechanical properties of SSC, which might contribute to the generation of $\text{Pdpn}^+\text{Grem1}^+\text{Ptgs2}^+$ SSC.

To explore the possible role of YAP activation in the SSC reprogramming towards immunomodulatory phenotype, verteporfin, a specific YAP inhibitor, was used to treat SSC in microgels. The data showed that the expression of *Ptgs2*, also known as COX2, and its major product PGE_2 [28] were significantly higher in the SSC with microgels group. Notably, the YAP inhibitor group (SSC with microgels + verteporfin) showed significant decreases of the expression of *Ptgs2* and PGE_2 (Fig. 6F, G, H). Additionally, immunofluorescence staining showing a co-expression of *Pdpn* or *Grem1* with *Ptgs2* confirmed that $\text{Pdpn}^+\text{Grem1}^+\text{Ptgs2}^+$ SSC were significantly increased in microgels-delivered SSC (Fig. 6I, J, K). These findings suggested that the enhanced mechanical properties of SSC were closely involved in the increased production of *Ptgs2* in microgels-delivered SSC.

Since the scRNA-seq data suggested that $\text{Pdpn}^+\text{Grem1}^+\text{Ptgs2}^+$ SSC had enhanced immunomodulatory capabilities with macrophage regulation (Fig. 5A and E), the immunomodulatory effects of microgels-delivered SSC on inflammatory macrophages were verified by using SSC culture medium from different culture conditions (Fig. 6L and M). Compared to the SSC medium group, macrophages in the SSC with microgels medium group exhibited significantly lower expression of inflammatory factors TNF- α and IL-1 β but higher expression of immunoregulatory factor IL-10. In addition, the immunomodulatory effect on macrophages of SSC was strikingly eliminated by blocking the mechanical stimulation of microgels-delivered SSC with YAP-specific inhibitor verteporfin, suggesting that the suppression on macrophages of microgels-delivered SSC was mediated by the mechanosensitive protein YAP and associated pathways. Moreover, the suppressive effect on macrophages was also significantly abolished by blocking the function of *Ptgs2* with COX2 inhibitor NS-398, indicating that *Ptgs2* played a major role in the immunomodulatory function of microgels-delivered SSC (Fig. 6L and M).

Collectively, the mechanical reprogramming effects of microgel carriers enhanced the immunomodulatory capacity of SSC by activating YAP and increasing *Ptgs2* expression.

3.6. Microgels-delivered SSC with activated mechanical property and enhanced immunomodulatory capacity contributed to the preventive effects on OA macrophage activation and osteo-chondral lesions

To explore the mechanism by which the mechanical properties of the microgels affect the immunomodulatory capacity of SSC and contributions to OA treatment, the SSC were pretreated by using YAP inhibitor (verteporfin) and COX2 inhibitor (NS-398), respectively (Fig. 7A and B).

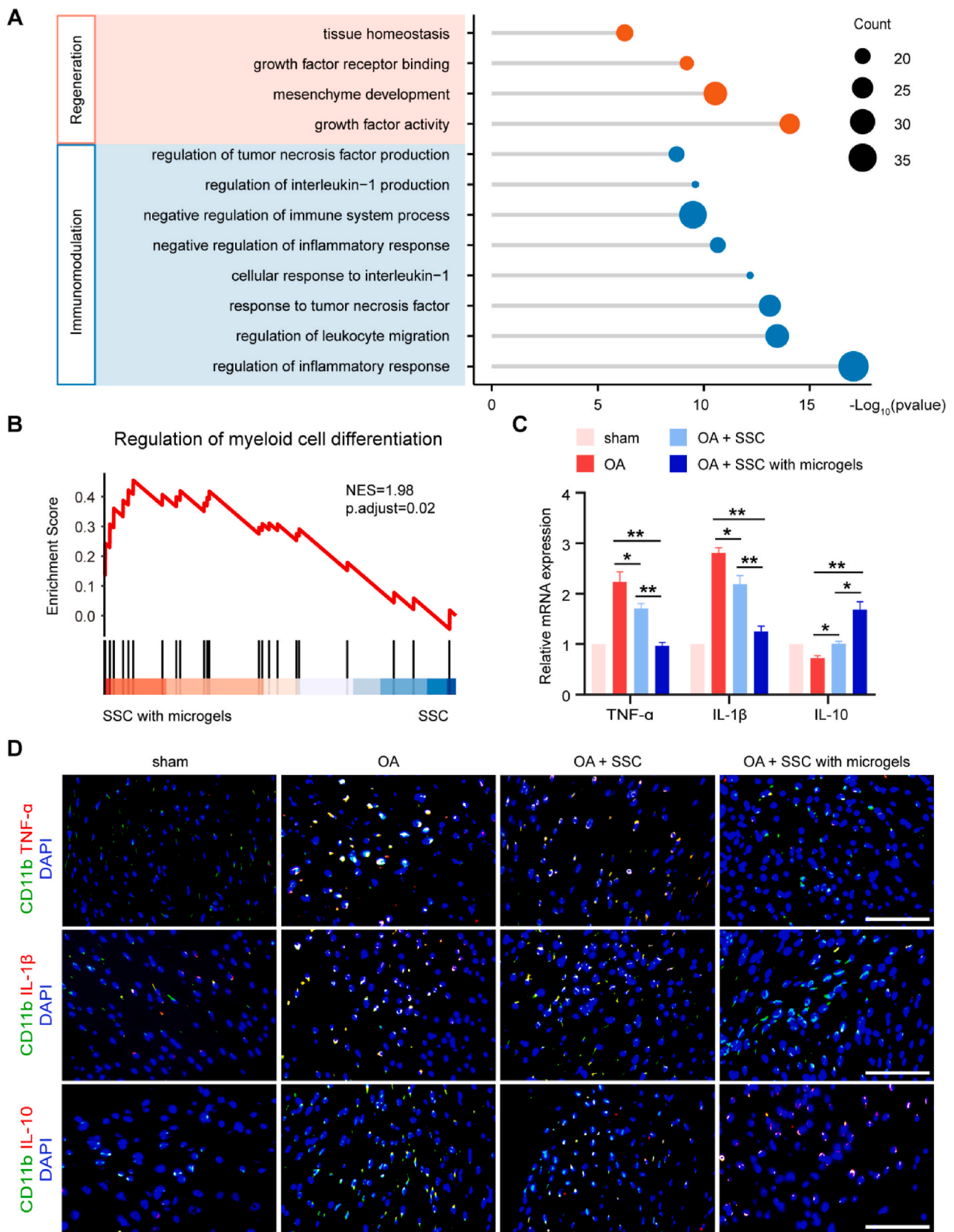


Fig. 3. The enhanced immunomodulatory capacity of SSC in microgel carriers. (A) Lollipop plot showing the representative GO terms enriched by significantly up-regulated genes in SSC with microgels. (B) GSEA analysis showing the enrichment of myeloid cell regulation function in SSC with microgels. NES = normalized enrichment score. (C) Relative mRNA expression of pro- and anti-inflammatory cytokines in the articular tissue of OA rats in different treatment groups. (D) Immunofluorescent staining showing the co-expression of TNF- α , IL-1 β , IL-10 with CD11b in the articular tissue of OA rats in different treatment groups. Nuclei are counterstained with DAPI. Scale bars: 50 μ m. All tests were replicated at least three times. * p < 0.05, ** p < 0.01. For the treatments of OA rats, $n \geq 5$ per group.

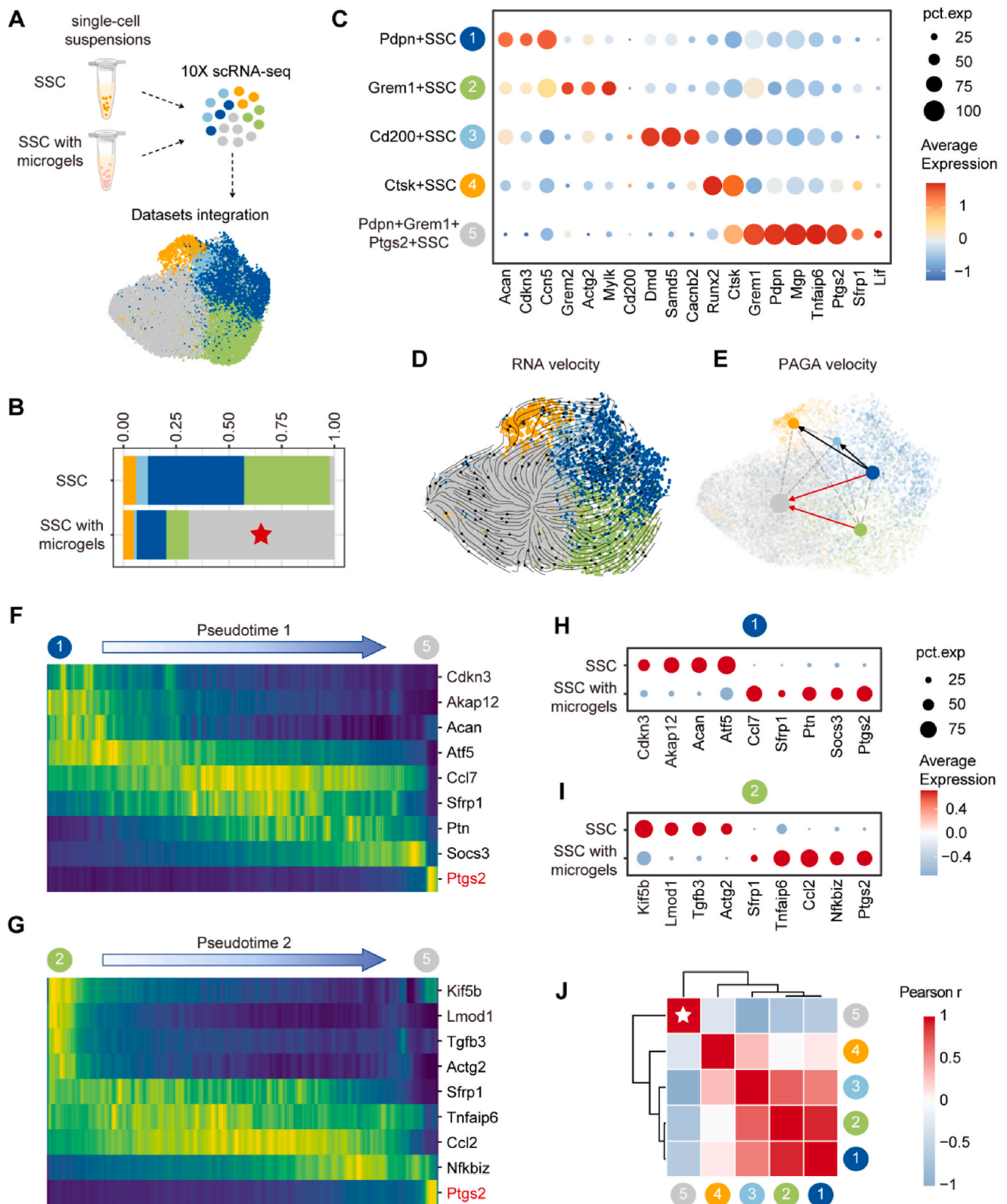


Fig. 4. Single-cell transcriptomic analyses of SSC in microgels. (A) Schematic illustration showing the integrated analysis of SSC scRNA-seq datasets with or without microgels. (B) Stacked bar graph showing the proportion of each subpopulation in SSC with or without microgels. SSC5 is marked with pentagram. (C) Dot plots showing the expression of feature genes in five subsets. The dot size represents the proportion of cells expressing specific genes and the dot color represents the expression level of genes. (D) Pseudotime trajectory inferred by RNA velocity on UMAP embeddings. (E) Partition-based graph abstraction (PAGA) mapping showing the connectivity among clusters. (F–G) Heatmap showing the expressions of 9 selected representative genes in Pdpn⁺ SSC, Grem1⁺ SSC and Pdpn⁺Grem1⁺Ptgs2⁺ SSC subsets ordered by pseudotime in (D) and (E). (H–I) Dot plot showing the expression of 9 representative genes in SSC with or without microgels along pseudotime trajectory 1 (H) and 2 (I). The dot size represents the proportion of cells expressing specific genes and the dot color represents the expression level of genes. (J) Pearson correlation analysis among 5 subsets. SSC5 is marked with pentagram.

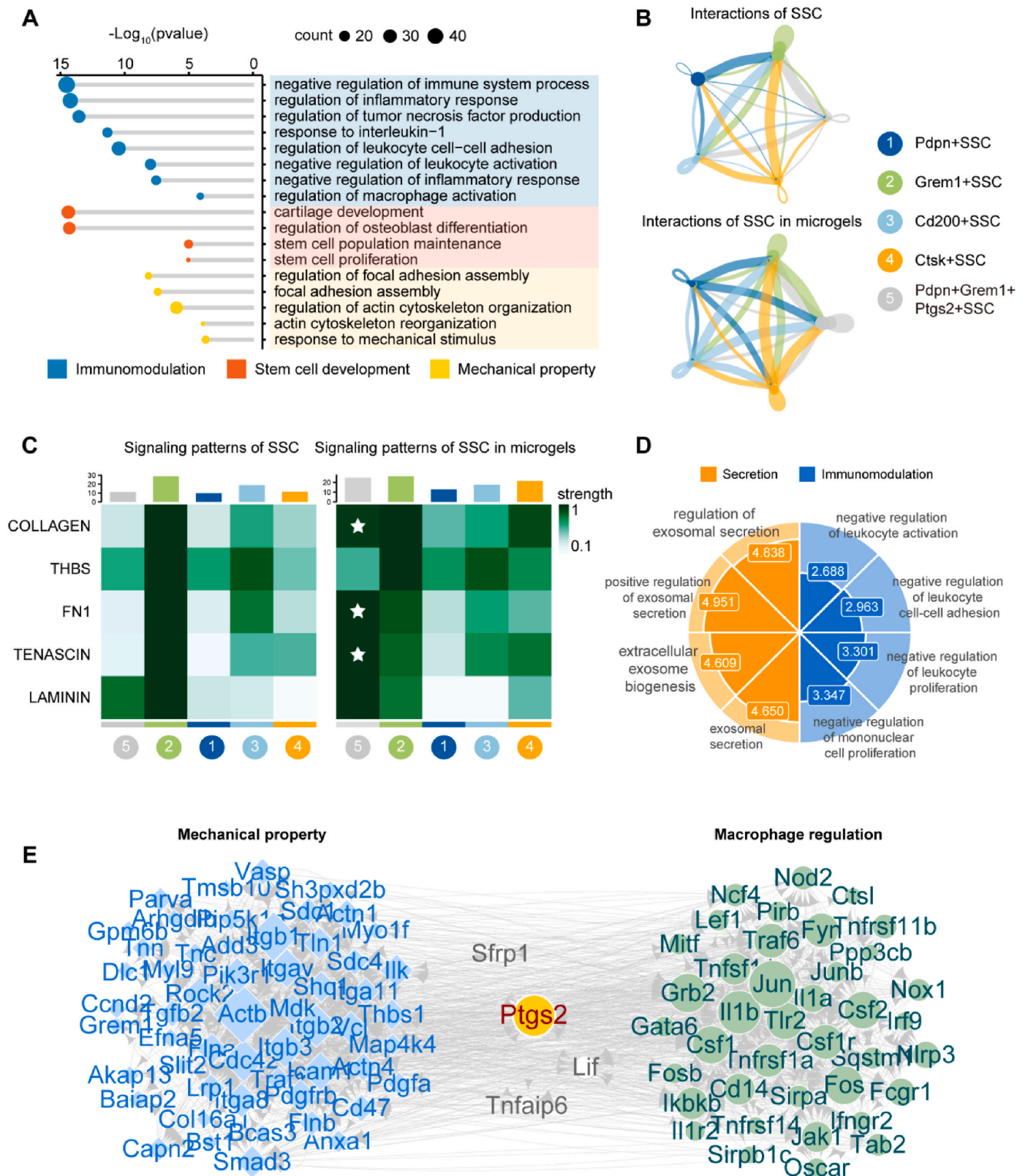
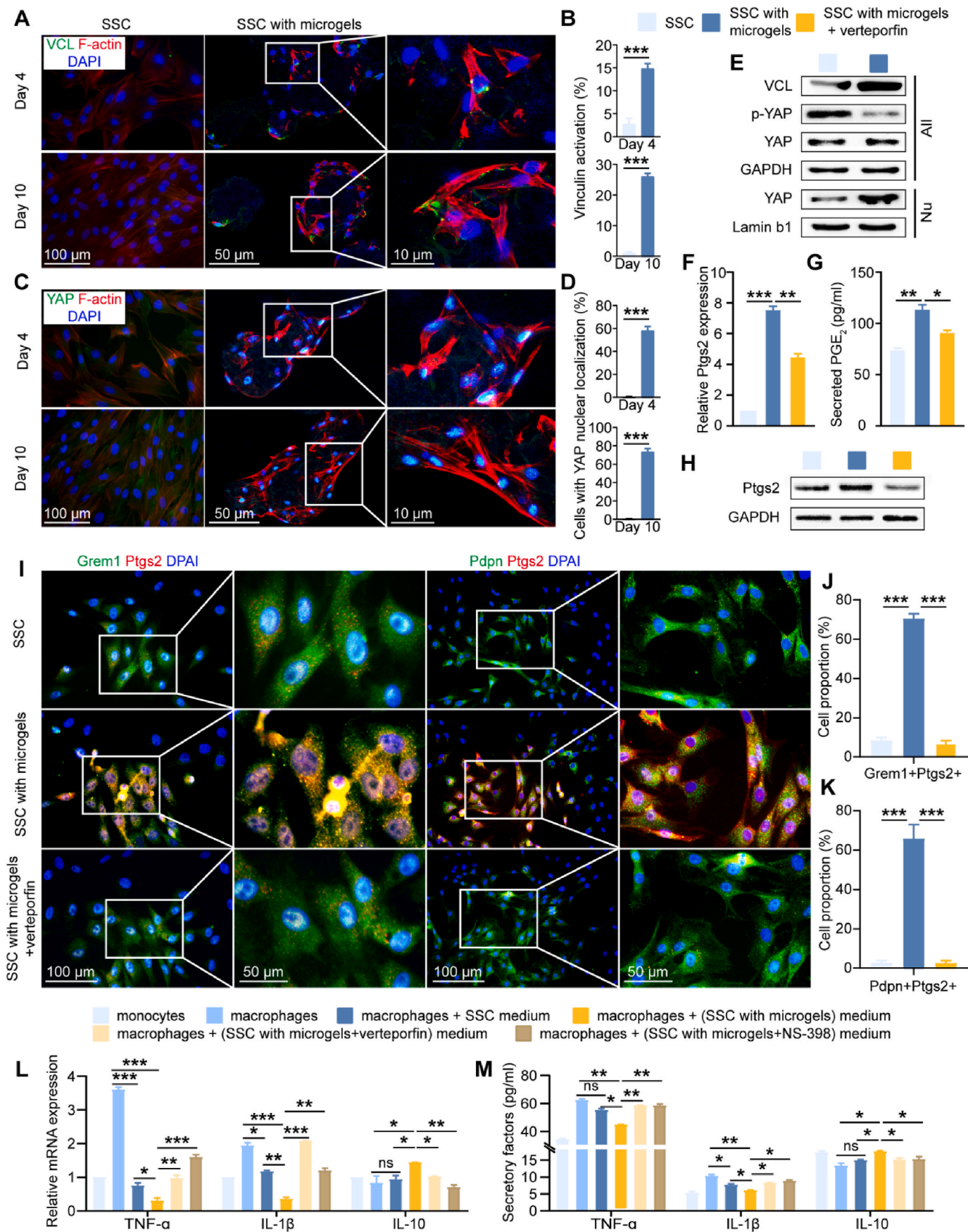


Fig. 5. Characteristics of Pdpn⁺ Grem1⁺Ptgs2⁺ SSC analyzed by scRNA-seq. (A) Lollipop plot showing the representative GO terms enriched by significantly up-regulated genes in Pdpn⁺Grem1⁺Ptgs2⁺ SSC. (B) CellChat analysis showing the “ECM-Receptor” signaling networks in SSC with or without microgels. Node size represents the number of cells in each subpopulation and edge thickness represents the weight of interaction. (C) Heatmap showing the most significant “ECM-Receptor” signaling pathways in SSC with microgels. Significant pathways in SSC with microgels are marked with pentagram. (D) Radar plot showing the representative GO terms enriched by the genes in the most significant “ECM-Receptor” ligand-receptor pairs. The number represents the $-\log_{10}(p\ value)$. (E) The interaction networks showing the correlation of representative immunomodulatory genes (*Sfrp1*, *Ptgs2*, *Lif* and *Tnfaip6*) in Pdpn⁺Grem1⁺Ptgs2⁺ SSC subset with mechanosensitive and macrophage regulation gene sets. The dot size represents the interaction strengths.



(caption on next page)

Fig. 6. Functional analysis of mechanical properties and Ptg2 expression in SSC with microgel carriers. (A) 3D confocal images of SSC with or without microgel carriers at days 4 and 10 after staining with vinculin (VCL) and F-actin. (B) The proportion of cells with vinculin activation in SSC with or without microgel carriers. (C) 3D confocal images of SSC with or without microgel carriers at 4 and 10 days after staining with YAP and F-actin. (D) The proportion of cells with nuclear localization of YAP in SSC with or without microgel carriers. (E) The total protein expression of VCL, phospho-YAP (p-YAP) and YAP in SSC with or without microgel carriers. GAPDH served as control; nuclear protein expression of YAP in SSC with or without microgel carriers. Lamin b1 served as control. (F) Relative mRNA expression of *Ptg2* in all groups. (G) Secretion of PGE_2 in all groups. (H) Total protein expression of *Ptg2* in all groups. (I) Immunofluorescence staining showing the co-expression of *Pdpn* or *Grem1* with *Ptg2* in all groups. (J) The proportion of cells co-expression of *Grem1* with *Ptg2* in all groups. (K) The proportion of cells co-expression of *Pdpn* with *Ptg2* in all groups. (L) Relative mRNA expression of pro- and anti-inflammatory cytokines in macrophages in all groups. (M) Secretion of pro- and anti-inflammatory cytokines by macrophages in all groups. All tests were replicated at least three times. * $p < 0.05$, ** $p < 0.01$, *** $p < 0.001$, ns, no significance.

The μCT data showed that the knee osteochondral damage was more severe in the SSC with microgels + verteporfin group and the SSC with microgels + NS-398 group compared with that of the SSC with microgels group (Fig. 7C). Quantitative analysis of μCT exhibited that OA grade was consistent with the changes in the μCT images (Fig. 7D), which suggested that blockage of YAP and *Ptg2* weakened the efficacy of SSC with microgels. Further histological analysis showed that the therapeutic effects of microgels-delivered SSC on osteochondral lesions were partially abolished after pretreatment with the two inhibitors, manifested by more cartilage destruction (Fig. 7E), higher Mankin score (Fig. 7F), lower expression of type II collagen (Fig. 7G), and higher expression of type I collagen (Figs. S10A and B). The results of immunofluorescence staining showed that compared with the SSC with microgels group, microgels-delivered SSC pretreated with verteporfin or NS-398 exhibited an increase of $\text{CD11b}^+\text{TNF-}\alpha^+$ and $\text{CD11b}^+\text{IL-1}\beta^+$ macrophages, but a decrease of $\text{CD11b}^+\text{IL-10}^+$ macrophages in the joint tissues of OA rats (Fig. 7H). Consistently, the qPCR results confirmed that the blockage of YAP and *Ptg2* of microgels-delivered SSC weakened the suppression on the expression of macrophage-derived inflammatory factors such as $\text{TNF-}\alpha$ and $\text{IL-1}\beta$, and reduced the expression of the anti-inflammatory factor such as IL-10 (Fig. 7I).

Together, these results demonstrated that microgels-delivered SSC exhibited enhanced immunomodulatory capacity by activating YAP and increasing *Ptg2* expression.

4. Discussion

MDSC are previously characterized by differentiating into stromal cells and synthesizing extracellular matrix so as to provide structural support for organs development, homeostasis and regeneration [29,30]. However, increasing studies showed that immune regulation of MDSC also significantly contributed to these processes. Mesenchymal stem cells (MSC) are one of the MDSC and are well known to participate in tissue homeostasis and regeneration [31–33]. In vitro expanded MSC have been demonstrated to have therapeutic potential for the settlement of immune disorders including graft versus host disease, Crohn's disease, and rheumatoid arthritis [34–36]. Our previous study demonstrates that MSC are capable of improving PLGA scaffold biocompatibility by inhibiting host dendritic cell maturation and function [37]. SSC is tissue specific MDSC in skeletons and is previously characterized by committedly osteochondrogenic capacity while OA progression cause generally skeletal degradation in joints. However, our findings confirmed that the generation of the immunomodulatory capacity of SSC within microgels, which yielded enhanced therapeutic effects on OA via suppressing overactivated macrophages.

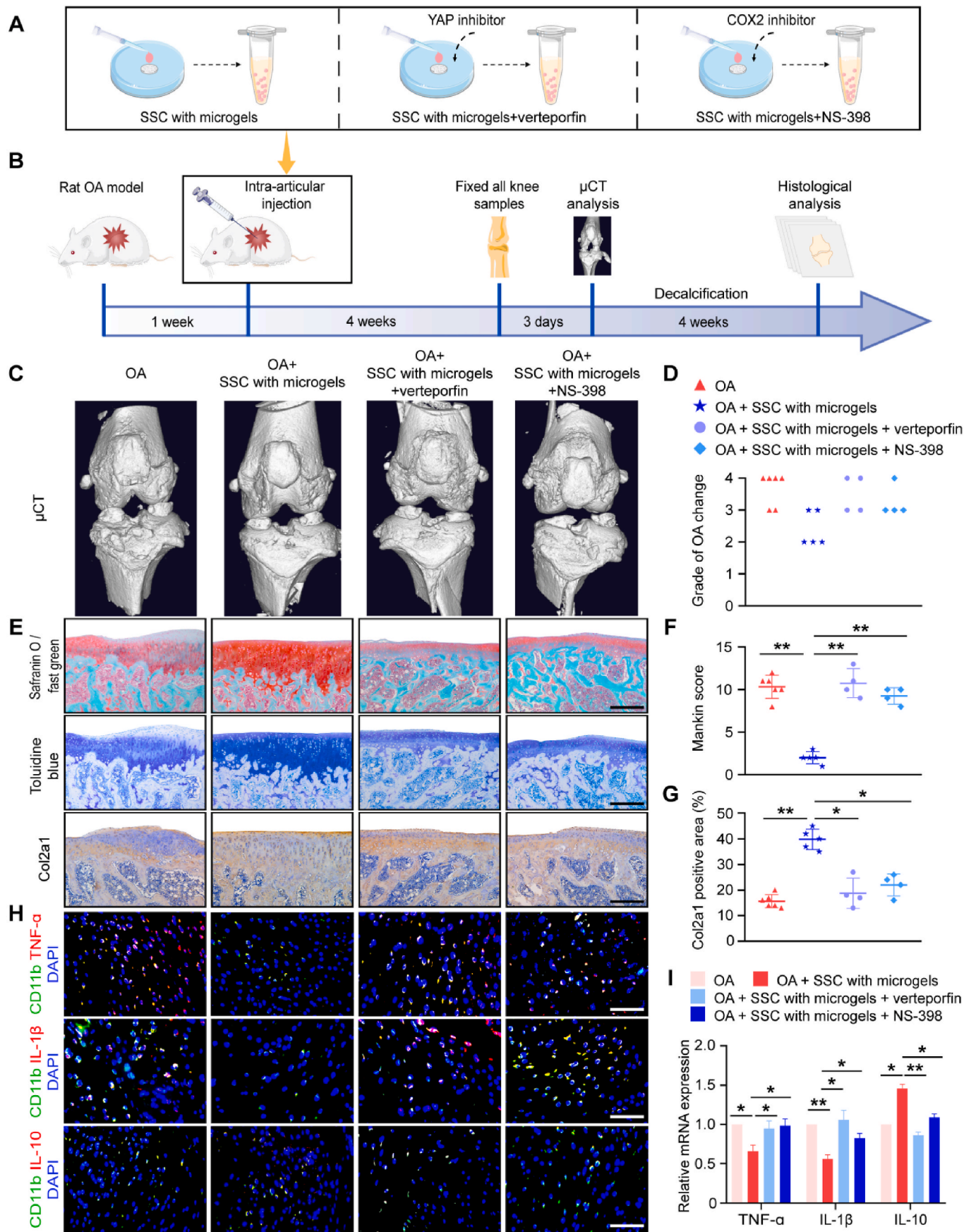
In the current study, the bulk RNA-seq data suggested that the SSC cultured in cell dishes could regulate innate immune response and suppressed leukocyte activation, while microgels-delivered SSC enhanced the suppression on $\text{TNF-}\alpha$ and $\text{IL-1}\beta$ production and response. Notably, the data showed that microgels delivery system facilitated SSC gained capacity to regulate myeloid cell differentiation. Although bulk RNA-seq analysis indicated the immunoregulatory potential and plasticity of SSC, it could not identify the cellular subpopulations in SSC and their possible alternation, which could contribute to the functional changes.

By advantage of scRNA-seq analysis, we acquired the unbiased profile of cellular subpopulations in SSC. The results showed that instead of the Cd200^+ and Cstk^+ subpopulations, the Pdpn^+ and Grem1^+ subpopulations have immunoregulatory potential in vitro expanded SSC, which suggested that the immunoregulatory potential are heterogeneous in SSC subpopulations. Further scRNA-seq data of SSC in microgels demonstrated that a novel $\text{Pdpn}^+\text{Grem1}^+\text{Ptgs2}^+$ subpopulation was generated from both Pdpn^+ and Grem1^+ subpopulation according to pseudotime analysis. These findings not only revealed the enhanced immunoregulation of SSC in microgels, but were also consistent with previous studies that delivery system might influence the immunoregulation of stem cells [38].

As has been reported, immunoregulatory genes, including IL-10 , IL-6 , *Ptg2*, $\text{TGF-}\beta$, TSG-6 , HGF and ICAM1 , are highly expressed in encapsulated MSC, which contributes to the immunomodulation of MSC [39]. However, the study just focuses on the overall immunomodulatory effects of MSC. Notably, the subpopulation alteration in stem cells has recently been revealed as novel cellular mechanism that controls tissue regeneration. Zhang et al. showed that tendon stem/progenitor cells delivered in gelatin microcarrier developed $\text{FGF7}^+\text{CYGB}^+$ and $\text{ICAM1}^+\text{ITGB8}^+$ subpopulations which promoted tendon repairing with improved tenogenic differentiation capacity [40]. This study demonstrated that cell-subpopulation alteration in response to the mechanical effects of microgels played a pivotal role in improving stem cell-mediated tissue regeneration. In the current study, our scRNA-seq analysis showed that SSC in microgels exhibited stronger self-renewal capacity compared with that of SSC in cell dishes. Importantly, we found the emergence of immunoregulatory $\text{Pdpn}^+\text{Grem1}^+\text{Ptgs2}^+$ subpopulation in microgels-delivered SSC.

We further investigated the immunoregulation of SSC *in vivo* by using OA models. According to the indication that SSC controlled macrophage activation by bioinformatics analysis and the *in vitro* effects of SSC medium on macrophage secretion of inflammatory factors, we hypothesized that the immunoregulation property at least partially accounted for SSC-mediated protection on OA joints. Previous studies attributed the regenerative capacity of SSC to differentiation into osteochondral cells [41]. In the current study, Sry immunofluorescence and bioluminescence imaging were performed to clarify the possibility of engraftment of intra-articularly injected SSC. The survival time of SSC in microgels *in vivo* was significantly longer than that of SSC without microgels; however, the microgels-delivered SSC yet could not be observed at day 12, which the time was limited to allow SSC to differentiate into osteochondral tissues. The Sry immunofluorescence data further demonstrated that no injected SSC was observed in the OA rat knees. In addition, blockage of the expression of *Ptg2* in microgels-delivered SSC significantly abolished the strengthen suppression on OA macrophage and impaired the better protection on joint tissues compared with SSC without microgels. Thus, these data suggested that SSC in microgels promoted tissue regeneration not by their limited differentiation potentials but their enhanced immunomodulation capacity to induce favorable immune microenvironment.

To explore whether the microgel carriers participated in controlling SSC immunomodulation, the activation of YAP in SSC with or without microgels were analyzed due to the pivotal role of YAP-mediated regulation on stem cells. Previous studies reported that



(caption on next page)

Fig. 7. YAP and its downstream COX2 mediated the efficacy of SSC with microgel carriers on osteoarthritic macrophages and osteochondral lesions in OA model. (A) Schematic illustration showing the pretreatment of SSC in microgels with YAP inhibitor (verteporfin) or COX2 inhibitor (NS-398). (B) Schematic illustration showing the treatment for rat OA with pretreated SSC in (A) and their therapeutic efficacy evaluation. (C) μ CT analysis of OA articular tissues in different treatment groups at 4 weeks after intra-articular injection. (D) OA grade change in each treatment group at 4 weeks after injection. (E) Safranin O/fast green staining (top), toluidine blue staining (middle) and Col2a1 immunohistochemical staining (bottom) of OA articular tissues in each treatment group at 4 weeks after injection. Scale bars: 200 μ m. (F) Mankin scores of each treatment group at 4 weeks after injection. (G) Semi-quantitative analysis of Col2a1 immunohistochemical staining for each treatment group at 4 weeks after injection. (H) Immunofluorescent staining showing the co-expression of TNF- α , IL-1 β , IL-10 with CD11b in the articular tissue of OA rats in different treatment groups. Nuclei are counterstained with DAPI. Scale bars: 50 μ m. (I) Relative mRNA expression of pro- and anti-inflammatory cytokines in the articular tissue of OA rats in different treatment groups. All tests were replicated at least three times. * $p < 0.05$, ** $p < 0.01$. For the treatments of OA rats, $n \geq 5$ per group.

mechanobiological conditioning could activate YAP signaling to promote stem cell proliferation [29,42]. In the current study, SSC delivered with microgels enhanced the intercellular communication, as well as the mechanical interaction between cells and extracellular matrix (ECM), thereby promoting the reorganization of the cytoskeleton and activating YAP signaling, shown as enhanced expression of vinculin, and increased YAP in cell nucleus. Blocking YAP in microgels-delivered SSC with a specific inhibitor significantly reduced the expression of Ptg2 and PGE₂, which had suppressive effects on inflammatory macrophages. Additionally, pretreatment of SSC in microgels with YAP inhibitor impaired the strengthened immunoregulation of SSC on macrophages in OA rats and the therapeutic effects on osteochondral lesions. Our findings first reported that the mechanical effects of microgels on the activation of YAP signaling in SSC, and the role of YAP in controlling SSC immunoregulation, which suggested microgels delivery technology and YAP-targeted strategy could be helpful to improve the immunoregulatory plasticity of SSC.

However, we acknowledge that some limitations remain present in the current study. First, although the *in vitro* expanded SSC have been demonstrated to have immunoregulatory potential and plasticity, and contribute to the prevention of OA osteochondral lesions, the immune properties of *in situ* SSC remain to be investigated in further studies. Second, the effects of SSC immunoregulation need to be clarified in more microenvironments such as tumorigenesis and autoimmune diseases. Third, the application of multiomics analysis in future studies will be helpful to reveal the underlying mechanisms that control SSC immunoregulation. Fourth, in the current study, rat SSC were used to exclude the possible influence of species, but the findings need to be validated in human SSC for future SSC-based therapy. Fifth, the chemical composition of materials used in the current study may inherently possess biological activity which influencing SSC subpopulation alteration and osteochondrogenic capacity *in vivo*. Although we focus on the potential role of mechanistic events such as YAP-translocation in SSC, the chemical factors of microgels on the SSC need to be explored in the future study. Sixth, the particle sizes of microgels may contribute to the underlying mechanisms of SSC reprogramming immunoregulatory capacity. Seventh, except for inflammatory cytokines, other factors including mechanistic factor may contribute to the microgels degradation *in vivo*.

5. Conclusion

In the study, we developed the delivery system for SSC with microgels for OA treatment. The immunoregulatory capacity of SSC, and the reprogramming effects mediated by microgel carriers on the SSC subpopulation alteration and immunomodulatory phenotype were investigated by single-cell transcriptomic and functional analysis at the first time. The single-cell transcriptomic characteristics of SSC defined the Pdpn⁺Grem1⁺Ptg2⁺ SSC as an immunoregulatory subpopulation. Further bioinformatic and functional analysis identified the indispensable role of microgel carriers in YAP activation for promoting SSC immunoregulatory capacity. The application of SSC in the treatment of experimental OA demonstrated that immunoregulation and their plasticity were pivotal properties of SSC that contributed to skeletal regeneration except for osteochondral differentiation. Moreover, microgel carriers also prolonged SSC retention time *in vivo* without increasing SSC

implanting into OA joints. In short, our study demonstrated the immunological mechanisms of SSC-based therapy at the single-cell level, as well as provided new insight for microgel carriers in stem cell-based therapy.

Conflict of interest disclosure

The authors declare that they have no competing interests.

Ethics approval statement

The animal research involved in this work was approved by the Institutional Animal Care and Use Committee of Military Medical Sciences (IACUC-DWZX-2020-765) on September 15, 2020.

Funding statement

This work was supported by the National Key R&D Program of China (Nos. 2022YFA1104100, 2022YFA1103500, 2022YFB3804400), the National Natural Sciences Grants China (Nos. 82172388, 82372373, 81871771, 52373128, 52273121), the Beijing Natural Sciences Foundation (Nos. 7222123, L212065, 7222011) and the Beijing Municipal Health Commission (Nos. BMHC-2021-6, BJRITO-RDP-2023).

Data availability statement

The datasets used and/or analyzed during the current study are available from the corresponding author on reasonable request.

CRediT authorship contribution statement

Pei-Lin Li: Writing – original draft, Visualization, Validation, Software, Resources, Methodology, Investigation, Formal analysis, Data curation. **Da-Fu Chen:** Writing – review & editing, Supervision, Project administration, Funding acquisition, Conceptualization. **Xiao-Tong Li:** Methodology, Investigation. **Rui-Cong Hao:** Methodology, Investigation. **Zhi-Dong Zhao:** Methodology, Investigation. **Zhi-Ling Li:** Methodology, Investigation. **Bo-Feng Yin:** Methodology, Investigation. **Jie Tang:** Methodology, Investigation. **Yu-Wen Luo:** Methodology, Investigation. **Chu-Tse Wu:** Writing – review & editing, Supervision, Project administration, Funding acquisition, Conceptualization. **Jing-Jun Nie:** Writing – review & editing, Visualization, Validation, Methodology, Investigation, Funding acquisition, Formal analysis, Data curation. **Heng Zhu:** Writing – review & editing, Writing – original draft, Visualization, Validation, Supervision, Project administration, Funding acquisition, Formal analysis, Data curation, Conceptualization.

Appendix A. Supplementary data

Supplementary data to this article can be found online at <https://doi.org/10.1016/j.bioactmat.2023.12.022>.

References

- [1] L. Sharma, Osteoarthritis of the knee, *N. Engl. J. Med.* 384 (1) (2021) 51–59.

- [2] I. Bernabei, A. So, N. Busso, S. Nasi, Cartilage calcification in osteoarthritis: mechanisms and clinical relevance, *Nat. Rev. Rheumatol.* 19 (1) (2023) 10–27.
- [3] J.P. Rhoads, A.S. Major, J.C. Rathmell, Fine tuning of immunometabolism for the treatment of rheumatic diseases, *Nat. Rev. Rheumatol.* 13 (5) (2017) 313–320.
- [4] W. Hu, Y. Chen, C. Dou, S. Dong, Microenvironment in subchondral bone: predominant regulator for the treatment of osteoarthritis, *Ann. Rheum. Dis.* 80 (4) (2021) 413–422.
- [5] P.G. Conaghan, A.D. Cook, J.A. Hamilton, P.P. Tak, Therapeutic options for targeting inflammatory osteoarthritis pain, *Nat. Rev. Rheumatol.* 15 (6) (2019) 355–363.
- [6] L.D. Sordo, G.B. Blackler, H.T. Philpott, J. Riviere, L. Gunaratnam, B. Heit, C. T. Appleton, Impaired efferocytosis by synovial macrophages in patients with knee osteoarthritis, *Arthritis Rheumatol.* 75 (5) (2023) 685–696.
- [7] R. Shkhyan, C. Flynn, E. Lamoure, A. Sarkar, B.V. Hande, J. Li, J. York, N. Banks, R. V. Horst, N.Q. Liu, S. Lee, P. Bajaj, K. Vadivel, H.I.C. Harn, J. Tasse, T. Lozito, J. R. Lieberman, C.M. Chuong, M.S. Hurtig, D. Evseenko, Inhibition of a signaling modality within the gp130 receptor enhances tissue regeneration and mitigates osteoarthritis, *Sci. Transl. Med.* 15 (688) (2023), eabq2395.
- [8] K. Zhou, C. Yang, K. Shi, Y. Liu, D. Hu, X. He, Y. Yang, B. Chu, J. Peng, Z. Zhou, Z. Qian, Activated macrophage membrane-coated nanoparticles relieve osteoarthritis-induced synovitis and joint damage, *Biomaterials* 295 (2023), 122036.
- [9] P.L. Li, Y.X. Wang, Z.D. Zhao, Z.L. Li, J.W. Liang, Q. Wang, B.F. Yin, R.C. Hao, M. Y. Han, L. Ding, C.T. Wu, H. Zhu, Clinical-grade human dental pulp stem cells suppressed the activation of osteoarthritic macrophages and attenuated cartilaginous damage in a rabbit osteoarthritis model, *Stem Cell Res. Ther.* 12 (1) (2021) 260.
- [10] J.M. Álvaro-Gracia, J.A. Jover, R. García-Vicuña, L. Carreño, A. Alonso, S. Marsal, F. Blanco, V.M. Martínez-Taboada, P. Taylor, C. Martín-Martín, O. DelaRosa, I. Tagarro, F. Díaz-González, Intravenous administration of expanded allogeneic adipose-derived mesenchymal stem cells in refractory rheumatoid arthritis (Cx611): results of a multicentre, dose escalation, randomised, single-blind, placebo-controlled phase Ib/IIa clinical trial, *Ann. Rheum. Dis.* 76 (1) (2017) 196–202.
- [11] C.K.F. Chan, E.Y. Seo, J.Y. Chen, D. Lo, A. McArdle, R. Sinha, R. Tevlin, J. Seita, J. Vincent-Tompkins, T. Wearda, W.J. Lu, K. Senarath-Yapa, M.T. Chung, O. Marecic, M. Tran, K.S. Yan, R. Upton, G.G. Walsley, A.S. Lee, D. Sahoo, C. J. Kuo, I.L. Weissman, M.T. Longaker, Identification and specification of the mouse skeletal stem cell, *Cell* 160 (1–2) (2015) 285–298.
- [12] D.L. Worthley, M. Churchill, J.T. Compton, Y. Tailor, M. Rao, Y. Si, D. Levin, M. G. Schwartz, A. Uygur, Y. Hayakawa, S. Gross, B.W. Renz, W. Setlik, A.N. Martínez, X. Chen, S. Nizami, H.G. Lee, H.P. Kang, J.M. Caldwell, S. Asfaha, C.B. Westphalen, T. Graham, G. Jin, K. Nagar, H. Wang, M.A. Kheirbek, A. Kolhe, J. Carpenter, M. Glaire, A. Nair, S. Renders, N. Manieri, S. Muthupalani, J.G. Fox, M. Reichert, A. S. Giraud, R.F. Schwabe, J.P. Pradere, K. Walton, A. Prakash, D. Gumucio, A. K. Rustgi, T.S. Stappenbeck, R.A. Friedman, M.D. Gershon, P. Sims, T. Grikscheit, F. Y. Lee, G. Karsenty, S. Mukherjee, T.C. Wang, Gremlin 1 identifies a skeletal stem cell with bone, cartilage, and reticular stromal potential, *Cell* 160 (1–2) (2015) 269–284.
- [13] C.K.F. Chan, G.S. Gulati, R. Sinha, J.V. Tompkins, M. Lopez, A.C. Carter, R. C. Ransom, A. Reinisch, T. Wearda, M. Murphy, R.E. Brewer, L.S. Koepke, O. Marecic, A. Manjunath, E.Y. Seo, T. Leavitt, W.J. Lu, A. Nguyen, S.D. Conley, A. Gahlotra, T.H. Ambrosi, M.R. Borrelli, T. Siebel, K. Chan, K. Schallmoser, J. Seita, D. Sahoo, H. Goodnough, J. Bishop, M. Gardner, R. Majeti, D.C. Wan, S. Goodman, I.L. Weissman, H.Y. Chang, M.T. Longaker, Identification of the human skeletal stem cell, *Cell* 175 (1) (2018) 43–56.
- [14] M.P. Murphy, L.S. Koepke, M.T. Lopez, X. Tong, T.H. Ambrosi, G.S. Gulati, O. Marecic, Y. Wang, R.C. Ransom, M.Y. Hoover, H. Steininger, L. Zhao, M. P. Walkiewicz, N. Quarto, B. Levi, D.C. Wan, I.L. Weissman, S.B. Goodman, F. Yang, M.T. Longaker, C.K.F. Chan, Articular cartilage regeneration by activated skeletal stem cells, *Nat. Med.* 26 (10) (2020) 1583–1592.
- [15] S. Menon, A. Salhotra, S. Shailendra, R. Tevlin, R.C. Ransom, M. Januszky, C.K. F. Chan, B. Behr, D.C. Wan, M.T. Longaker, N. Quarto, Skeletal stem and progenitor cells maintain cranial suture patency and prevent craniosynostosis, *Nat. Commun.* 12 (1) (2021) 4640.
- [16] Y. Li, W. Liu, F. Liu, Y. Zeng, S. Zuo, S. Feng, C. Qi, B. Wang, X. Yan, A. Khademhosseini, J. Bai, Y. Du, Primed 3D injectable microniches enabling low-dose cell therapy for critical limb ischemia, *Proc. Natl. Acad. Sci. U.S.A.* 111 (37) (2014) 13511–13516.
- [17] F. Zhang, L. Wang, Y. Li, W. Liu, F. Duan, R. Huang, X. Chen, S.C.N. Chang, Y. Du, J. Na, Optimizing mesoderm progenitor selection and three-dimensional microniche culture allows highly efficient endothelial differentiation and ischemic tissue repair from human pluripotent stem cells, *Stem Cell Res. Ther.* 8 (1) (2017) 6.
- [18] H. Zhu, Z.K. Guo, X.X. Jiang, H. Li, X.Y. Wang, H.Y. Yao, Y. Zhang, N. Mao, A protocol for isolation and culture of mesenchymal stem cells from mouse compact bone, *Nat. Protoc.* 5 (3) (2010) 550–560.
- [19] S. Jiang, C. Lyu, P. Zhao, W. Li, W. Kong, C. Huang, G.M. Genin, Y. Du, Cryoprotectant enables structural control of porous scaffolds for exploration of cellular mechano-responsiveness in 3D, *Nat. Commun.* 10 (1) (2019) 3491.
- [20] J.E. Kim, S.M. Lee, S.H. Ki, P. Tatman, A.O. Gee, D.H. Kim, K.E. Lee, Y. Jung, S. J. Kim, Effect of self-assembled peptide-mesenchymal stem cell complex on the progression of osteoarthritis in a rat model, *Int. J. Nanomed.* 9 (Suppl 1) (2014) 141–157.
- [21] M. Rahimi, G. Charmi, K. Matyjaszewski, X. Banquy, J. Pietrasik, Recent developments in natural and synthetic polymeric drug delivery systems used for the treatment of osteoarthritis, *Acta Biomater.* 123 (2021) 31–50.
- [22] I.A. Jones, R. Togashi, M.L. Wilson, N. Heckmann, C.T.V. Jr, Intra-articular treatment options for knee osteoarthritis, *Nat. Rev. Rheumatol.* 15 (2) (2019) 77–90.
- [23] H. Zhang, D. Cai, X. Bai, Macrophages regulate the progression of osteoarthritis, *Osteoarthritis Cartilage* 28 (5) (2020) 555–561.
- [24] J. Xie, Z. Huang, X. Yu, L. Zhou, F. Pei, Clinical implications of macrophage dysfunction in the development of osteoarthritis of the knee, *Cytokine Growth Factor Rev.* 46 (2019) 36–44.
- [25] S. Debnath, A.R. Yallowitz, J. McCormick, S. Lalani, T. Zhang, R. Xu, N. Li, Y. Liu, Y.S. Yang, M. Eisman, J.H. Shim, M. Hameed, J.H. Healey, M.P. Bostrom, D. A. Landau, M.B. Greenblatt, Discovery of a periosteal stem cell mediating intramembranous bone formation, *Nature* 562 (7725) (2018) 133–139.
- [26] R. Moreno-Vicente, D.M. Pavón, I. Martín-Padura, M. Catalá-Montoro, A. Díez-Sánchez, A. Quilez-Álvarez, J.A. López, M. Sánchez-Álvarez, J. Vázquez, R. Strippoli, M.A.D. Pozo, Caveolin-1 modulates mechanotransduction responses to substrate stiffness through actin-dependent control of YAP [published correction appears in *Cell Rep.* 25 (6) (2018) 1622–1635].
- [27] S. Li, C. Li, Y. Zhang, X. He, X. Chen, X. Zeng, F. Liu, Y. Chen, J. Chen, Targeting mechanics-induced fibroblast activation through CD44-RhoA-YAP pathway ameliorates crystalline silica-induced silicosis, *Theranostics* 9 (17) (2019) 4993–5008.
- [28] J.Y. Park, M.H. Pillinger, S.B. Abramson, Prostaglandin E2 synthesis and secretion: the role of PGE2 synthases, *Clin. Immunol.* 119 (3) (2006) 229–240.
- [29] H. Soliman, M. Theret, W. Scott, L. Hill, T.Mi Underhill, B. Hinz, F.M.V. Rossi, Multipotent stromal cells: one name, multiple identities, *Cell Stem Cell* 28 (10) (2021) 1690–1707.
- [30] A.I. Caplan, Mesenchymal stem cells: time to change the name, *Stem Cells Transl Med* 6 (6) (2017) 1445–1451.
- [31] R.W. Scott, M. Arostegui, R. Schweitzer, F.M.V. Rossi, T.M. Underhill, Hic1 defines quiescent mesenchymal progenitor subpopulations with distinct functions and fates in skeletal muscle regeneration, *Cell Stem Cell* 25 (6) (2019) 797–813.
- [32] H. Soliman, B. Paylor, R.W. Scott, D.R. Lemos, C.K. Chang, M. Arostegui, M. Low, C. Lee, D. Fiore, P. Braghetta, V. Pospichalova, C.E. Barkauskas, V. Korinek, A. Rampazzo, K. MacLeod, T.M. Underhill, F.M.V. Rossi, Pathogenic potential of hic1-expressing cardiac stromal progenitors, *Cell Stem Cell* 26 (2) (2020) 205–220.
- [33] A.C. Habermann, A.J. Gutierrez, L.T. Bui, S.L. Yahn, N.H. Winters, C.L. Calvi, L. Peter, M.I. Chung, C.J. Taylor, C. Jetter, L. Raju, J. Roberson, G. Ding, L. Wood, J.M.S. Sucre, B.W. Richmond, A.P. Serezani, W.J. McDonnell, S.B. Mallal, M. J. Bacchetta, J.E. Loyd, C.M. Shaver, L.B. Ware, R. Bremner, R. Walia, T. S. Blackwell, N.E. Banovich, J.A. Kropski, Single-cell RNA sequencing reveals profibrotic roles of distinct epithelial and mesenchymal lineages in pulmonary fibrosis, *Sci. Adv.* 6 (28) (2020), eaba1972.
- [34] A.J.C. Bloor, A. Patel, J.E. Griffin, M.H. Gilleece, R. Radia, D.T. Yeung, D. Drier, L. S. Larson, G.I. Unish, D. Hei, K. Kelly, I. Slukvin, J.E.J. Rasko, Production, safety and efficacy of iPSC-derived mesenchymal stromal cells in acute steroid-resistant graft versus host disease: a phase I, multicenter, open-label, dose-escalation study, *Nat. Med.* 26 (11) (2020) 1720–1725.
- [35] J. Panés, D. García-Olmo, G.V. Assche, J.F. Colombel, W. Reinisch, D.C. Baumgart, A. Dignass, M. Nachury, M. Ferrante, L. Kazemi-Shirazi, J.C. Grimaud, F.d. I. Portilla, E. Goldin, M.P. Richard, A. Leselbaum, S. Danese, ADMIRE CD Study Group Collaborators, Expanded allogeneic adipose-derived mesenchymal stem cells (Cx601) for complex perianal fistulas in Crohn's disease: a phase 3 randomised, double-blind controlled trial, *Lancet* 388 (10051) (2016) 1281–1290.
- [36] J.M. Álvaro-Gracia, J.A. Jover, R. García-Vicuña, L. Carreño, A. Alonso, S. Marsal, F. Blanco, V.M. Martínez-Taboada, P. Taylor, C. Martín-Martín, O. DelaRosa, I. Tagarro, F. Díaz-González, Intravenous administration of expanded allogeneic adipose-derived mesenchymal stem cells in refractory rheumatoid arthritis (Cx611): results of a multicentre, dose escalation, randomised, single-blind, placebo-controlled phase Ib/IIa clinical trial, *Ann. Rheum. Dis.* 76 (1) (2017) 196–202.
- [37] H. Zhu, F. Yang, B. Tang, X.M. Li, Y.N. Chu, Y.L. Liu, S.G. Wang, D.C. Wu, Y. Zhang, Mesenchymal stem cells attenuated PLGA-induced inflammatory responses by inhibiting host DC maturation and function, *Biomaterials* 53 (2015) 688–698.
- [38] A.S. Mao, B. Özkale, N. J. Shah, K.H. Vining, T. Descombes, L. Zhang, C. M. Tringides, S.W. Wong, J.W. Shin, D.T. Scadden, D.A. Weitz, D.J. Mooney, Programmable microencapsulation for enhanced mesenchymal stem cell persistence and immunomodulation, *Proc. Natl. Acad. Sci. U.S.A.* 116 (31) (2019) 15392–15397.
- [39] K. Carter, H.J. Lee, K.S. Na, G.M. Fernandes-Cunha, I.J. Blanco, A. Djalilian, D. Myung, Characterizing the impact of 2D and 3D culture conditions on the therapeutic effects of human mesenchymal stem cell secretome on corneal wound healing in vitro and ex vivo, *Acta Biomater.* 99 (2019) 247–257.
- [40] H. Zhang, Y. Chen, C. Fan, R. Liu, J. Huang, Y. Zhang, C. Tang, B. Zhou, X. Chen, W. Ju, Y. Zhao, J. Han, P. Wu, S. Zhang, W. Shen, Z. Yin, X. Chen, H. Ouyang, Cell-subpopulation alteration and FGF7 activation regulate the function of tendon stem/progenitor cells in 3D microenvironment revealed by single-cell analysis, *Biomaterials* 280 (2022), 121238.
- [41] J.W. Liang, P.L. Li, Q. Wang, S. Liao, W. Hu, Z.D. Zhao, Z.L. Li, B.F. Yin, N. Mao, L. Ding, H. Zhu, Ferulic acid promotes bone defect repair after radiation by maintaining the stemness of skeletal stem cells, *Stem Cells Transl Med* 10 (8) (2021) 1217–1231.
- [42] X. Zhang, D. Cao, L. Xu, Y. Xu, Z. Gao, Y. Pan, M. Jiang, Y. Wei, L. Wang, Y. Liao, Q. Wang, L. Yang, X. Xu, Y. Gao, S. Gao, J. Wang, R. Yue, Harnessing matrix

stiffness to engineer a bone marrow niche for hematopoietic stem cell rejuvenation, *Cell Stem Cell* 30 (4) (2023) 378–395.